Langmuir Article

pubs.acs.org/Langmuir

Dual-Emitting Langmuir−Blodgett Film-Based Organic Light-Emitting Diodes

Henk J. Bolink,*[,†,§] Etienne Baranoff,[‡] Miguel Clemente-León,*[,†,§] Eugenio Coronado,[†] Nora Lardiés,[†] Angel López-Muñoz,[†] Diego Repetto,[†] and Md. K. Nazeeruddin[‡]

[†]*Instituto de Ciencia Molecular, Universidad de Valencia, calle catedrático José Beltrán 2, 46980 Paterna, Spain,* [‡]*Laboratory for Photonics and Interfaces, Ecole Polytechnique Fédérale de Lausanne, CH-1015 Lausanne, Switzerland, and* [§]*Fundació General de la Universitat de València (FGUV), Spain*

Received March 9, 2010. Revised Manuscript Received May 5, 2010

Langmuir−Blodgett (LB) films containing alternating layers of the metallosurfactants bis(4,4′-tridecyl-2,2′-bipyridine)-(4,4′-dicarboxy-2,2′-bipyridine) ruthenium(II)-bis(chloride) (**1**) and bis[2-(2,4-difluorophenyl)pyridine](4,4′-dinonadecyl-2,2′-bipyridine)iridium(III) chloride (**2**) have been prepared. Langmuir monolayers at the air−water interface of **1** and **2** with different anions in the subphase have been characterized by $\pi-A$ compression isotherms and Brewster angle microscopy (BAM). The transferred LB films have been characterized by IR, UV−vis and emission spectroscopy, and atomic force microscopy (AFM). Electroluminescent devices formed by LB films containing alternating layers of these two molecules show dual emission by simple mixing of the two emitters in a single LB film, and by preparing two stacked configurations, in which a LB layer of the ruthenium complexes is deposited on top of a LB layer of the iridium complexes and the inverse situation. The color of the electroluminescence can be tuned by changing the thickness of each LB layer. Due to efficient hole blocking of a layer of the iridium complexes when deposited on top of the layer of ruthenium complexes, in that configuration the green emission of the iridium complexes is suppressed. In the opposite case, excitons are generated in both layers although most likely preferentially in the layer of the iridium complexes.

Introduction

The Langmuir−Blodgett (LB) technique is a well-established method to control interfacial molecular orientation and packing. Furthermore, it is an efficient approach toward the controllable fabrication of well-organized multilayered films with a very precise control of the thickness and composition, that is not available with other techniques.[1] This technique has been widely applied to create ultrathin films with a specific architecture, which can be used as chemical sensors, modified electrodes, or molecular electronic devices.[1,2] There are many examples of the use of this technique to prepare emissive,[3] hole-injection,[4] or insulating layers[5] for organic light-emitting diodes (OLEDs). Most of these examples are based on neutral polymers, although a few of them are based on the use of metal complexes.[3c,e]

In the past few years, the preparation of efficient white OLEDs has generated significant interest for solid-state lighting applications, due to potential savings in both cost and energy use.[6] Many white light emission devices are obtained by sequential evaporation of the active materials under high vacuum conditions which involves high energy consumption and hence high costs. In addition, emitter stability issues have been observed with this process.[7] In the search for simple and stable processing and low cost devices, it is desirable to use large area compatible solution based processes. However, the number of sequential layers that can be obtained using solution based processes is limited due to redissolving of the underlying layers. Recently, however, some reports were made of sequential layer deposition using a single solvent with a doctor blade technique.[8] The amount of intermixing that might occur on a nanoscale is, however, not easily determined. This can have a significant influence on the performance of light-emitting devices as demonstrated recently by Kido et al.[9] The use of the LB technique can overcome some of the potential problems of intermixing layers, as it affords a better control of the layer thickness and permits very easily growth of alternating multilayers of different molecules. This can be useful from a fundamental point of view to understand the energy-transfer mechanisms that govern the behavior of the device.

To test this concept, we have chosen two metallosurfactants containing Ru and Ir, bis(4,4′-tridecyl-2,2′-bipyridine)-(4,4′-dicarboxy-2,2′-bipyridine) ruthenium(II)-bis(chloride) (**1**) and bis[2-(2,4-difluorophenyl)pyridine](4,4′-dinonadecyl-2,2′-bipyridine)iridium(III) chloride (**2**) (see Chart 1). These two compounds present the amphiphilic character needed to prepare LB films, emit at different wavelengths, and present efficient electronic energy transfer as shown recently in micelles formed by similar metallosurfactants.[10]

*To whom correspondence should be addressed. E-mail: henk.bolink@uv.es; miguel.clemente@uv.es.

(1) Ulman, A. *An Introduction to Ultrathin Organic Films from Langmuir−Blodgett to Self-Assembly*; Academic Press: San Diego, 1991.

(2) Talham, D. R. *Chem. Rev.* **2004**, *104*, 5479.

(3) (a) Olivati, C. A.; Péres, L. O.; Wang, S. H.; Giacometti, J. A.; Oliveira, O. N.; Balogh, D. T. *J. Nanosci. Nanotechnol.* **2008**, *8*, 2432. (b) Olivati, C. A.; Ferreira, M.; Carvalho, A. J. F.; Balogh, D. T.; Oliveira, O. N.; von Seggern, H.; Faria, R. F. *Chem. Phys. Lett.* **2005**, *408*, 31. (c) Yam, V. W. W.; Li, B.; Yang, Y.; Chu, B. W. K.; Wong, K. M. C.; Cheung, K. K. *Eur. J. Inorg. Chem.* **2003**, 4035. (d) Jung, G. Y.; Arias-Marin, E.; Arnault, J. C.; Guillon, D.; Maillou, T.; Le Moigne, J.; Geffroy, B.; Nunzi, J. M. *Langmuir* **2000**, *16*, 4309. (e) Ouyang, J.; Li, L.; Tai, Z.; Lu, Z.; Wang, G. *Chem. Commun.* **1997**, 815.

(4) (a) Xu, J.; Yang, Y.; Yu, J.; Jiang, Y. *Appl. Surf. Sci.* **2009**, *255*, 4329. (b) Aoki, A.; Maeda, S. N.; Kawai, Y.; Tanaka, T.; Miyashita, T. *Chem. Lett.* **2005**, *34*, 1566.

(5) (a) Jung, G. Y.; Pearson, C.; Horsburgh, L. E.; Samuel, I. D. W.; Monkman, A. P.; Petty, M. C. *J. Appl. Phys. D* **2000**, *33*, 1029. (b) Kim, Y. E.; Park, H.; Kim, J. J. *Appl. Phys. Lett.* **1996**, *69*, 599.

(6) (a) Sun, Y.; Giebink, N. C.; Kanno, H.; Ma, B.; Thompson, M. E.; Forrest, S. R. *Nature* **2006**, *440*, 908. (b) D'Andrade, B. W.; Forrest, S. R. *Adv. Mater.* **2004**, *16*, 1585.

(7) (a) Sivasubramaniam, V.; Brodkorb, F.; Hanning, S.; Loebl, H. P.; van Elsbergen, V.; Boerner, H.; Scherf, U.; Kreyenschmidt, M. *J. Fluorine Chem.* **2009**, *130*, 640. (b) Baranoff, E.; Suàrez, S.; Bugnon, P.; Barolo, C.; Buscaino, R.; Scopelliti, R.; Zuppiroli, L.; Graetzel, M.; Nazeeruddin, Md. K. *Inorg. Chem.* **2008**, *47*, 6575.

(8) Tseng, S. R.; Meng, H. F.; Lee, K. H.; Horng, S. F. *Appl. Phys. Lett.* **2008**, *93*, 153308/1.

(9) Su, S. J.; Gonmori, E.; Sasabe, H.; Kido, J. *Adv. Mater.* **2008**, *20*, 4189.

(10) Guerrero-Martínez, A.; Vida, Y.; Domínguez-Gutiérrez, D.; Albuquerque, R. Q.; De Cola, L. *Inorg. Chem.* **2008**, *47*, 9131.

Chart 1. Molecular Structure of 1, 2, and pTPD

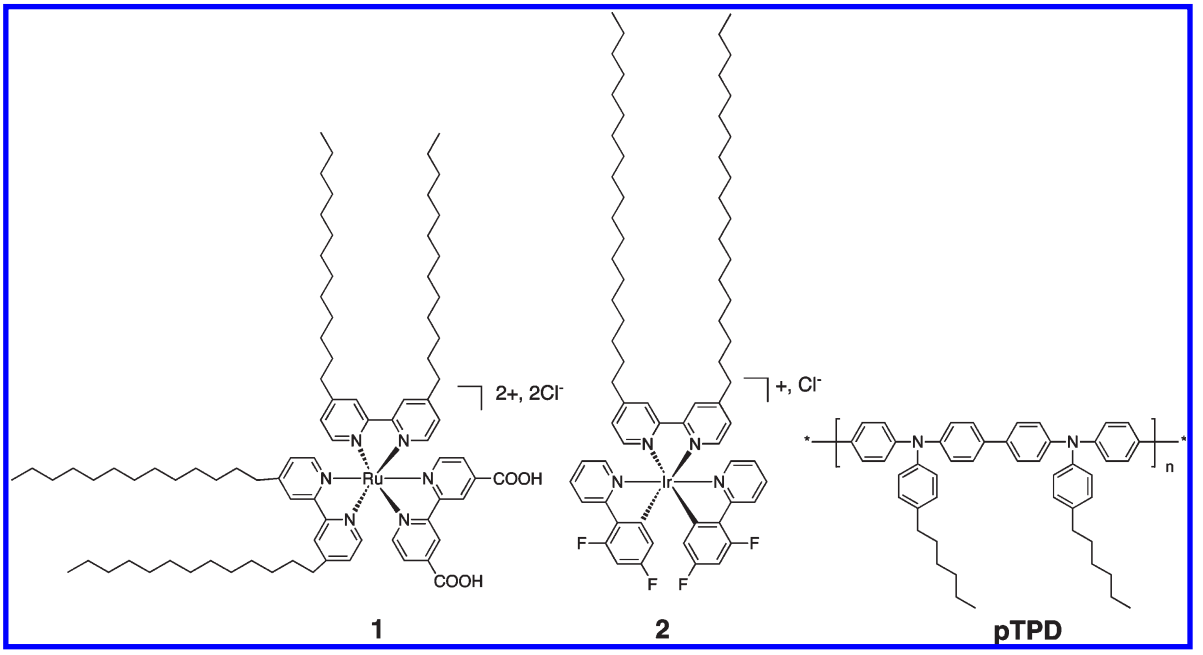

We have successfully prepared electroluminescent devices formed by LB films containing alternating layers of these two molecules. We have shown that, by controlling the disposition of these layers, it is possible to tune the color of the electroluminescence.

Experimental Section

1 was prepared as reported in the literature.[11] Poly(*N*,*N*′-diphenyl-*N*,*N*′-bis(4-hexylphenyl))-[1,1′-biphenyl]-4,4′-diamine (pTPD) and $H_4SiW_{12}O_{40}$ were obtained, respectively, from American Dye Source and Sigma and used without further purification.

Preparation of bis[2-(2,4-difluorophenyl)pyridine](4,4′-dinonadecyl-2,2′-bipyridine)iridium(III) chloride (**2**) is similar to that of other analogous compounds reported in the literature:[12] 4,4′-dinonadecyl-2,2′-bipyridine (152 mg, 0.22 mmol) and tetrakis(2-(2,4-diflfluorophenyl)pyridine)-μ-(dichloro)-diiridium(III) (122 mg, 0.1 mmol) in 5 mL of ethylene glycol were refluxed overnight. The resulting brown-yellow solid was suspended in water, filtered, and washed with ethanol and water. The complex was further purified by recrystallization in a mixture of 3 mL of dichloromethane and 25 mL of acetonitrile in the freezer. A first brown precipitate that appeared after a few hours was discarded. A yellow precipitate was obtained after a few days in the mother liquor.

^{1}H NMR (300 MHz, $CDCl_3$): δ (ppm) = 9.32 (s, 2H); 8.32 (d, 2H, J = 3.3 Hz); 7.81 (t, 2H, J = 6.9 Hz); 7.72 (d, 2H, J = 5.7 Hz); 7.52 (d, 2H, J = 6 Hz); 7.23 (d, 2H, J = 6 Hz); 7.10 (t, 2H, J = 7 Hz); 6.55 (d, 2H, J = 2.1 Hz); 5.68 (d, 2H, J = 2.4 Hz); 2.98 (t, 4H); 1.71 (S, 16H); 1.25 (m, 60H); 0.87 (t, 12H). ^{19}F NMR (300 MHz, $CDCl_3$): δ (ppm) = −136 (d); −139 (d). MS (ESI), m/z (%): 1262 ($[M]^+$, 100%); 1010 ($[M - (CH_2)_{18}]^+$, 72%).

A solution of **1**, **2**, or a mixture of both compounds in $CHCl_3$ was used as spreading solution. An appropriate amount of these solutions was carefully spread onto a 10^{-6} M $H_4[SiW_{12}O_{40}]$ aqueous subphase for **1**, pure water for **2**, and 10^{-3} M KPF_6 aqueous subphase for **1** and **2** mixtures. After spreading, the solvent was allowed to evaporate for 10 min prior to compression. The monolayer was compressed up to a surface pressure of 30 mN m^{-1} for transfer of **1**, 24 mN/m for transfer of **2**, and 14 mN/m for transfer of **1** and **2** mixtures. The LB films were assembled to the substrate by the vertical lifting method, that is, immersion and withdrawal of the substrate through the interface covered with the charged complex monolayer. The dipping speed of the substrates was 1 cm min^{-1}. Isotherms were obtained with a NIMA trough (type 702BAM) equipped with a Wilhelmy plate and maintained at 20 °C. A KSV3000 trough was used to prepare the LB films. Millipore water with a resistivity higher than 18 MΩ cm was used in all the experiments. A EP^3-BAM from NFT was used for the brewster angle microscopy (BAM) experiments.

Infrared (IR) spectra were recorded on a FTIR 320 Nicolet spectrometer in transmission mode using a bare substrate as reference. UV−vis spectra were recorded on a Shimadzu UV-2401PC spectrometer. Emission spectra were measured on a Hamamatsu, model C9920-01 with a Xenon/Mercury-Xenon lamp. A commercial Atomic Force Microscope (AFM) (Multimode SPM by Veeco) was employed for surface sample characterization. The microscope was operated in tapping mode using commercial super sharp tips (nominal tip radius 2 nm, max 5 nm) and 0.01−0.025 Ωcm Antimony (n) doped Si cantilevers (L:110−140 μm, W:25−35 μm, f:320−400 kHz, k:20−80 N/m). AFM images were processed by using WSxM 5.0.[13]

Devices were prepared by spin-coating a thin layer (80 nm) of the pTPD from a chlorobenzene solution on the indium tin oxide (ITO) covered glass substrates. Before spin-coating, the solutions were filtered over a 0.20 μm poly(tetrafluoroethylene) (PTFE) filter. The spin-coated films were annealed at 150 °C for 10 min. Afterward, the LB films were transferred on the ITO/pTPD substrate. Then, the thin films were dried and transferred into a high vacuum chamber integrated in an inert atmosphere (< 0.1 ppm O_2 and H_2O) glovebox. Ba (5 nm) and then Ag (70 nm) were thermally evaporated under a base pressure of 10^{-6} mbar serving as the anode contact and as an optical mirror to enhance the unidirectional light output of the device. The layer thickness was determined using an Ambios XP1 profilometer. $J-V$ characteristics were collected using a Keithley 2400 source measurement unit. Electroluminescence was detected using a Si-photodiode coupled to a Keithley 6485 picoamperometer. The photocurrent was calibrated using a Minolta LS100 luminance meter. Electroluminescent spectra were recorded using an Avantes fiber optics photospectrometer.

(11) Bolink, H. J.; Baranoff, E.; Clemente-León, M.; Coronado, E.; López-Muñoz, A.; Repetto, D.; Sessolo, M.; Nazeeruddin, Md. K. *Langmuir* **2009**, *25*, 79.
(12) Lowry, M. S.; Hudson, W. S. *J. Am. Chem. Soc.* **2004**, *126*, 14129.
(13) Horcas, I.; Fernández, R.; Gómez-Rodríguez, J. M.; Colchero, J.; Gómez-Herrero, J.; Baro, A. M. *Rev. Sci. Instrum.* **2007**, *78*, 013705.

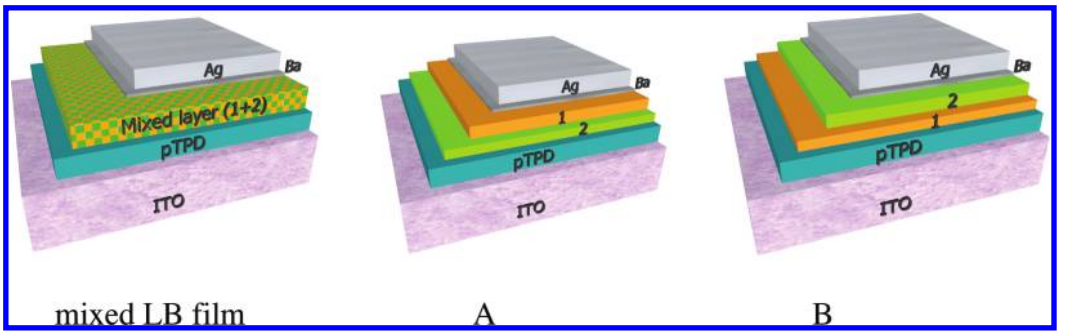

Figure 1. Architecture of the three types of devices prepared in this paper.

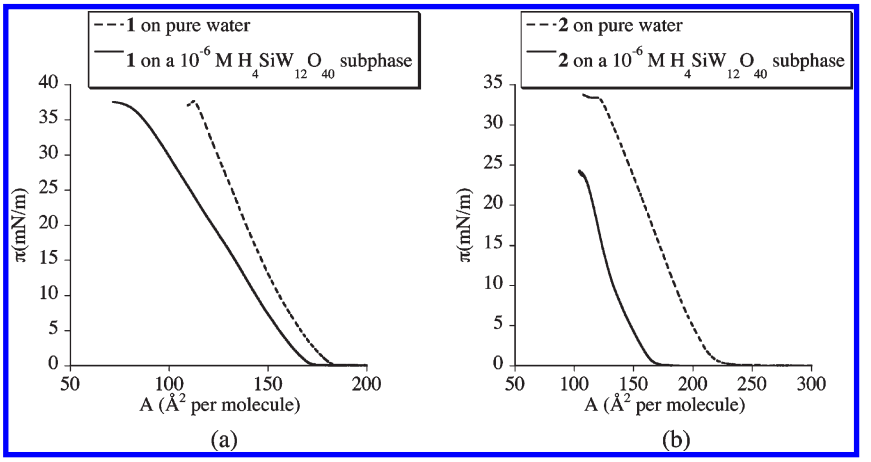

Figure 2. (a) Compression isotherms of monolayers of **1** on pure water and a on a subphase containing 10^{-6} M $H_4SiW_{12}O_{40}$. (b) Compression isotherms of **2** on pure water.

Results and Discussion

The architectures of the devices used in this paper are reported in Figure 1. The standard device configuration is as follows: glass substrates containing a patterned layer of 100 nm ITO, 80 nm of the hole-injection layer of pTPD, 30−40 monolayers of LB film of **1** and **2** in different configurations, and 5 nm Ba capped with 70 nm of Ag.

It was not possible to use poly(3,4-ethylenedioxythiophene) (PEDOT) stabilized with poly(styrene sulfonic acid) (PSS) as a charge injection layer due to the detaching of this material from the ITO covered substrates upon immerging in water that prevents the successive deposition of the emitting layer by the LB technique. Instead of PEDOT/PSS, a layer of 80 nm of pTPD was deposited by spin-coating. The presence of this layer is necessary to avoid the formation of shorts. The conductivity of unoxidized pTPD is around 10^{-8} S cm^{-1}. This conductivity may be increased to 0.01 S cm^{-1} by oxidizing with the Mn cluster $[Mn_{12}O_{12}(C_6F_5COO)_{16}]$, abbreviated as Mn_{12}.[14] This pTPD/Mn_{12} constitutes a promising hole-injection material. However, in our case, the devices were prepared on a pure pTPD layer for simplicity and to have a better reproducibility for the comparison between the various devices. The pTPD layer needed an annealing treatment to avoid detachment from the substrate upon submerging in the water subphase used for the subsequent LB transfer.

LB films of the complexes **1** and **2** at various compositions were deposited on top of the annealed pTPD layer (see Figure 1). The preparation of LB films of **1** was reported by our group in a recent paper.[11] We showed that monolayers of **1** deposited by the LB technique onto a TiO_2 cathode led to injection improvement in an organic electroluminescent device. For this work, we changed the preparation conditions by using a 10^{-6} M aqueous subphase of the $H_4SiW_{12}O_{40}$ polyoxometalate in place of the KPF_6 subphase from the previous work, as it increased the stability of the device and improved the LB formation (see below). LB films of **2** were prepared for the first time in this work on a pure water subphase. In this case, the use of a subphase containing small anions such as Cl^-, PF_6^-, or polyanions such as $[SiW_{12}O_{40}]^{4-}$ did not result in an improvement of the device. In the following section, we report the behavior of monolayers of **1** and **2** at the air−water interface, which is the first step for the LB film preparation.

Preparation of Monolayers. *π−A Isotherms*. Figure 2a shows the surface pressure−area (π−A) isotherms of **1** on pure water and spread on a subphase containing 10^{-6} M $H_4SiW_{12}O_{40}$ polyanion. The presence of $H_4SiW_{12}O_{40}$ in the subphase causes a shift of the isotherm toward smaller areas per molecule, which is more important at higher surface pressures. This indicates that the adsorption of the anions counterbalance the repulsions between the positively charged **1** molecules, leading to more compact monolayers as observed for positively charged surfactants such as DODA.[15] The collapse pressure is similar in both isotherms (around 37 mN/m). The area per molecule of **1** on a 10^{-6} M $H_4SiW_{12}O_{40}$ subphase at 30 mN/m is close to the calculated area of the $[Ru(bpy)_3]^{2+}$ unit (1 nm^2).[16] This suggests a compact packing of the **1** complexes at the air−water interface with the alkyl chains perpendicular to the water surface. At higher surface pressures, close to the collapse pressure, the areas per molecule are too small for a monolayer of **1**. This could indicate the formation of multilayers in part of the film.

(14) Bolink, H. J.; Cappelli, L.; Coronado, E.; Recalde, I. *Adv. Mater.* **2006**, *18*, 920.

(15) Clemente-León, M.; Coronado, E.; Gómez-García, C. J.; Mingotaud, C.; Ravaine, S.; Romualdo-Torres, G.; Delhaès, P. *Chem.—Eur. J.* **2005**, *11*, 3979.

(16) Vergeer, F. W.; Chen, X.; Lafolet, F.; De Cola, L.; Fuchs, H.; Chi, L. *Adv. Funct. Mater.* **2006**, *16*, 625.

The compression isotherm of **2** on pure water is shown in Figure 2b. It presents a smooth increase with large areas per molecule ranging from 220 Å^2/molecule at the beginning of the compression to 120 Å^2/molecule close to the collapse. These values are higher than those found for **1** complex. This indicates that **2** monolayer does not present a highly packed organization. A possible explanation is the electrostatic repulsion between the positively charged **2** molecules and a tilting of the alkyl chains due to the hydrophobicity of the C−F bonds of the fluorinated phenylpyridine ligands. The effect of the presence of polyanions such as $[SiW_{12}O_{40}]^{4-}$ is similar to that observed for **1** monolayer. The isotherm of the monolayer on a water subphase containing the polyanions is shifted toward smaller areas per molecule, but at the same time the collapse pressure is decreased with respect to that of the monolayer on a pure water subphase. This indicates again that the adsorption of anions counterbalances the repulsions between the positively charged **2** molecules, leading to more compact monolayers. However, as this is accompanied by a lower stability of the monolayer and a worse transfer onto solid substrates (see below), we decided to use a pure water subphase for the devices containing LB films of **2**.

Monolayers of mixtures of **1** and **2** were prepared in order to obtain close contacts between the two complexes within the built-up films. The miscibility of these two molecules was checked first by recording the compression isotherm of mixed **1**/**2** monolayers at various compositions (see Figure 1SS in the Supporting Information). A 10^{-3} M PF_6^- subphase was used as the presence of anions seems to improve the behavior of devices containing **1**. On the other hand, a $[SiW_{12}O_{40}]^{4-}$ subphase was not used as it induces a worse transfer of **2**. Figure 2SS in the Supporting Information shows as an example the change in mean molecular area at a surface pressure of 10 mN/m with the composition. The variation is not linear with the mole fraction of **2**. Furthermore, the collapse pressures of the mixed films depend on the composition of the monolayer. These results indicate that **1** and **2** are miscible components in a Langmuir monolayer.

Brewster Angle Microscopy (BAM). The monolayers of **1** and **2** were observed directly by BAM at the air−water interface to obtain information about the morphological properties of the different films. In the two cases, BAM images show homogeneous monolayers. BAM images of **1** monolayer are shown in the Supporting Information (Figure 3SS). At very low surface pressure, a homogeneous phase covers the whole surface (see image at π = 0.1 mN/m and 175 Å^2/molecule). The reflectivity of this monolayer is higher than that of the **1** monolayer on a pure water subphase. This effect may be related to the adsorption of the $[SiW_{12}O_{40}]^{4-}$ polyanions dissolved in the water subphase onto the **1** monolayer as shown by other positively charged monolayers in the presence of polyoxometalates.[17] At increasing surface pressure, there is an increase of the reflectivity over the entire surface. At surface pressures close to the collapse, a brighter band appears (see image at π = 36.0 mN/m and 84 Å^2/molecule). This could correspond to the formation of multilayer domains, explaining the low area per molecule values observed in the compression isotherm (see above). BAM images of the **2** monolayer on pure water are shown in the Supporting Information (Figure 4SS). When the monolayer is compressed, a brighter continuous domain is observed on a darker background (see image at π=0 mN/m and 219 Å^2/molecule). Under further compression, the brighter phase covers the whole surface (see image at 0.1 mN/m and 207 Å^2/molecule). Higher surface pressures lead to an increase of the reflectivity over the entire surface and to the onset of some brighter points close to the collapse (see image at 30 mN//m and 133 Å^2/molecule). We can conclude that BAM images indicate that **1** and **2** molecules form homogeneous monolayers at the air−water interface.

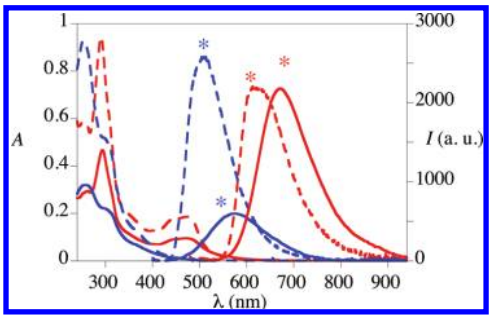

Figure 3. UV−vis and emission spectra of a LB films of **1** on a 10^{-6} M $H_4[SiW_{12}O_{40}]$ subphase with 29 monolayers deposited on a quartz substrate (red solid line), a 5×10^{-5} M $CHCl_3$ solution of **1** (red dashed line), LB film of **2** with 23 monolayers deposited on a quartz substrate (blue solid line), and a 1.2×10^{-5} M $CHCl_3$ solution of **2** (blue dashed line). Emission spectra in solution were performed on air-equilibrated samples. Emission spectra are marked with an asterisk.

LB films: Structural Characterization. LB Films of **1** were successfully deposited by the vertical lifting method at a constant surface pressure of 30 mN/m on a 10^{-6} M $H_4[SiW_{12}O_{40}]$ subphase. These LB films were prepared on both hydrophilic and hydrophobic substrates. The transfer ratio was close to unity for both immersion and withdrawal processes, indicating the formation of centrosymmetric Y-type LB films. In the case of monolayers of complex **2** on the same polyoxometalate subphase, transfer was only possible for the withdrawal of the substrate. Transfer ratios close to 0 were observed for the immersion of the substrate. This indicates the formation of noncentrosymmetric Z-type LB films. When a pure water subphase was used instead of the 10^{-6} M $H_4[SiW_{12}O_{40}]$ subphase, transfer ratios around 0.6−0.7 were obtained for both immersion and withdrawal processes at 24 mN/m. This suggests the formation of centrosymmetric Y-type LB films with incomplete coverage of the surface for each monolayer. This was confirmed by AFM images, and the thickness calculated by means of a profilometer (see below).

UV−Vis spectroscopy and Emission Properties. Figure 3 shows the UV−vis absorption spectrum of a LB film of **1** on a 10^{-6} M $H_4[SiW_{12}O_{40}]$ subphase with 29 monolayers together with that of a 5×10^{-5} M $CHCl_3$ solution of **1**. It shows two absorption bands at 294 and 471 nm typical of **1** ruthenium complex. The bands in the UV are mainly π−π* ligand centered (^{1}LC) transitions of the bipyridine ligands, while those at 471 with a shoulder at 430 nm are attributed to spin-allowed singlet metal-to-ligand charge transfer (^{1}MLCT) transitions.[10] The bands associated with the polyoxometalate cannot be detected due to the overlap with the characteristic bands of **1** in the UV. IR spectra (see below) demonstrate the presence of $[SiW_{12}O_{40}]^{4-}$ polyanions within the transferred LB films. This LB film shows, under excitation at 470 nm, a broad emission with a maximum around 670 nm from a state resulting from the ^{3}MLCT transition. It is red-shifted with respect to the emission of a diluted $CHCl_3$ solution of **1** (maximum at 627 nm) and with respect to the emission of analogous compounds in solution or forming micelles (Figure 3).[10,18] The UV−vis absorption spectrum of a LB film of **2** with 23 monolayers deposited on a quartz substrate together with that of a 1.2×10^{-5} M $CHCl_3$ solution of **2** is shown in Figure 3. It shows the absorption bands typical of iridium complex

(17) Cuvillier, N.; Bernon, R.; Doux, J. C.; Merzeau, P.; Mingotaud, C.; Delhaès, P. *Langmuir* **1998**, *14*, 5573.

(18) Lafolet, F.; Welter, S.; Popovic, Z.; De Cola, L. *J. Mater. Chem.* **2005**, *15*, 2820.

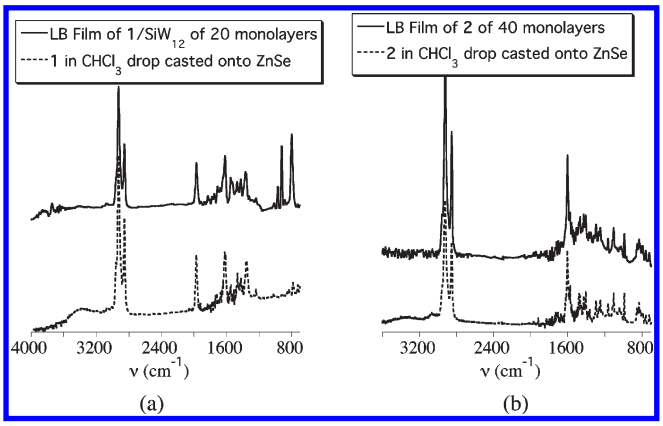

Figure 4. (a) IR spectra of **1** in $CHCl_3$ drop-casted onto ZnSe and a LB film of **1** on a 10^{-6} M $H_4[SiW_{12}O_{40}]$ subphase (20 ML deposited on ZnSe). (b) IR spectra of **2** in $CHCl_3$ drop-casted onto ZnSe and a LB film of **2** (40 ML deposited on ZnSe).

2, namely, an intense band at 256 nm with shoulders at 300 and 366 nm. The bands between 240 and 300 nm can be assigned to singlet spin-allowed $\pi-\pi^*$ ligand centered (^{1}LC) transitions of both fluorinated phenylpyridine and bipyridine ligands, while the bands between 300 and 360 can be assigned to Ir-based spin-allowed metal-to-ligand charge transfer (^{1}MLCT) transitions.[18] The room temperature emission spectrum of this LB film under excitation at 305 nm shows a peak around 570 nm from a state resulting from the mixing of ^{3}MLCT and ^{3}LC states. It is red-shifted with respect to the emission of a $CHCl_3$ solution of **2** (maximum at 510 nm) and with respect to the emission of an analogous compound in diluted water solution (maximum at 544 nm).[10]

The position of the bands associated to **1** or **2** in the absorption spectra is almost identical to that found in solution besides small differences of only 2−4 nm. This confirms the successful deposition of **1** and **2**. On the other hand, the organization of these molecules into LB films induces important changes in the emission wavelengths of the two complexes. This is related to the different environments of the complexes in solution and within the LB films. Probably these changes are due to the presence of aggregates with close packed Ir(III) and Ru(II) complexes. This increases the polarity of the local environment shifting the emission to the red in the same way as it occurs in solution when polar solvents are used. Polar solvents stabilize the excited estates more efficiently.[19]

Infrared Spectroscopy. The infrared (IR) spectrum of a LB film of 20 monolayers (ML) of **1** on a 10^{-6} M $H_4[SiW_{12}O_{40}]$ subphase deposited onto ZnSe is very similar to that of **1** drop-casted onto a ZnSe substrate or in KBr pellet (see Figure 4a). It is characterized by the bands at 2924, 2852, and 1470 cm^{-1} assigned to the CH_2 stretching or scissoring vibrations of the alkyl chains, the bands at 1547 and 1420 cm^{-1} assigned to the aromatic rings, and the bands at 1710 and 1328 cm^{-1} assigned to C═O and C−O stretching bands of the carboxylic acid. Two strong bands at 1618cm^{-1} ($-COO^-_{as}$) and 1363 cm^{-1} ($-COO^-_{s}$) could be assigned to the asymmetric and the symmetric stretching of the carboxylate group.[20] This indicates that **1** is at least partially deprotonated. Despite the net neutral charge of the deprotonated compound, the IR spectrum shows five strong bands below 1200 cm^{-1}, characteristic of the $[SiW_{12}O_{40}]^{4-}$ polyanion (see Figure 4a).

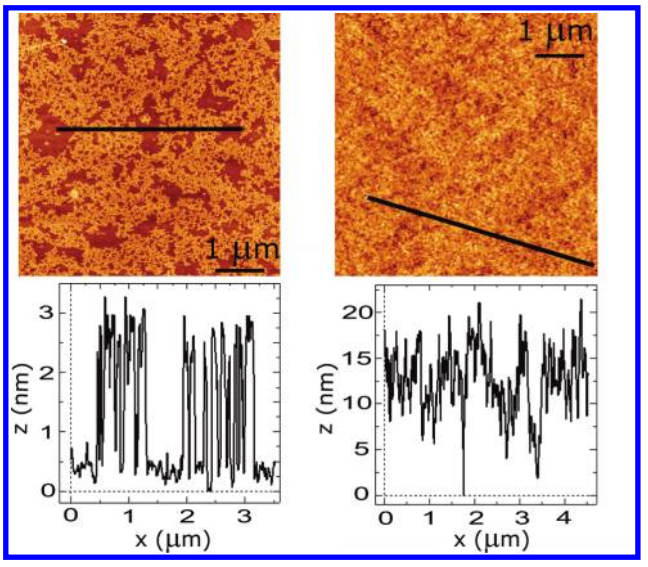

Figure 5. AFM images of LB films of **1** with 1 (left) and 9 (right) monolayers (ML) prepared on a 10^{-6} M $H_4SiW_{12}O_{40}$ water subphase deposited on a glass substrate. Image size: 5 μm × 5 μm.

This demonstrates the adsorption of the polyanions dissolved in the water surface onto the **1** monolayer and the subsequent transfer into the LB films as already observed with other polyoxometalates onto positively charged and zwitterionic surfactants.[15,21−23]

The infrared (IR) spectrum of a LB film of 40 ML of **2** deposited onto ZnSe is very similar to that of an evaporated $CHCl_3$ solution on a ZnSe substrate (see Figure 4b). It presents the bands at 2921, 2851, and 1464 cm^{-1} assigned to the CH_2 stretching or scissoring vibrations of the alkyl chains, the bands at 1602, 1576 1428, 1404, and 987 cm^{-1} assigned to the C−N and C−C bonds of the aromatic rings and two bands at 1165 and 1103 cm^{-1} assigned to the C−F bonds of **2**. We can conclude that the IR spectra of the LB films on ZnSe substrates confirms the successful deposition of **1** and **2** and the presence of $[SiW_{12}O_{40}]^{4-}$ counterions in the LB films of **1**. IR spectra of LB films of monolayers of mixed **1** and **2** onto a 10^{-3} M KPF_6 subphase present the bands characteristic of **1**, **2** and PF_6^- (see Figure 5SS, Supporting Information).

Atomic Force Microscopy. This technique has been used to complete the structural characterization and have a direct surface imaging of these LB films. LB films of **1** and **2** of different thickness deposited onto glass substrates have been studied by AFM.

A characteristic AFM image of a LB film of **1** on a 10^{-6} M $H_4[SiW_{12}O_{40}]$ subphase formed by one dipping cycle is shown in Figure 5. A flat bottom surface (rms roughness ~ 0.2 nm) corresponding to the naked substrate is mostly covered by a discontinuous film of average height around 2.3 nm. This value is consistent with the thickness of a monolayer of **1**. This indicates that the transfer is not perfect and that the first monolayer does not completely cover the surface. Furthermore, the absence of higher domains excludes the transfer of multilayers of **1** that were observed at the air−water interface at higher surface pressures by BAM. The deposition of a higher number of monolayers (see AFM image of a LB film of 9 ML, Figure 5) leads to an increase in height differences and, as a consequence, in the roughness (rms roughness ~ 3 nm). However,

(19) Domínguez-Gutiérrez, D.; De Paoli, G.; Guerrero-Martínez, A.; Ginocchietti, G.; Ebeling, D.; Eiser, E.; De Cola, L.; Elsevier, C. J. *J. Mater. Chem.* **2008**, *18*, 2762.
(20) Nazeeruddin, M. K.; Di Censo, D.; Humphry-Baker, R.; Grätzel, M. *Adv. Funct. Mater.* **2006**, *16*, 189.
(21) Clemente-Leon, M.; Agricole, B.; Mingotaud, C.; Gómez-García, C. J.; Coronado, E.; Delhaes, P. *Langmuir* **1997**, *13*, 2340.
(22) Clemente-León, M.; Coronado, E.; Soriano-Portillo, A.; Mingotaud, C.; Dominguez-Vera, J. M. *Adv. Colloid Interface Sci.* **2005**, *116*, 193.
(23) Clemente-León, M.; Coronado, E.; López-Muñoz, A.; Repetto, D.; Ito, T.; Konya, T.; Yamase, T.; Constable, E. C.; Housecroft, C. E.; Doyle, K.; Graber, S. *Langmuir* **2010**, *26*, 1316.

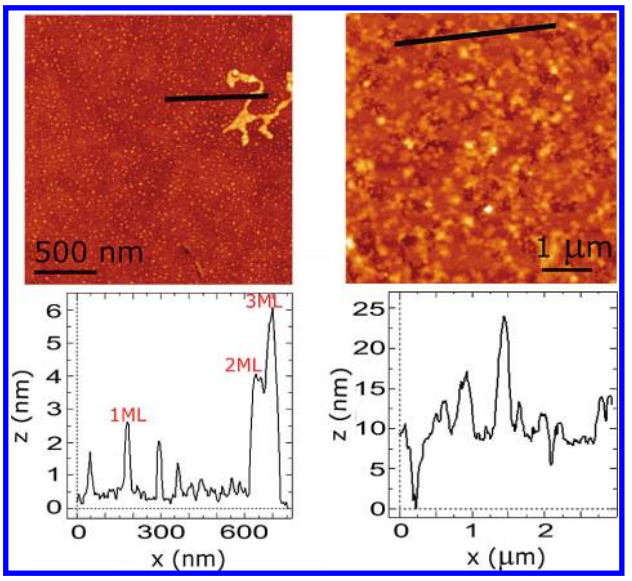

Figure 6. AFM images of LB films of **2** with 1 and 9 monolayers (ML) deposited on a glass substrate. Left image size: 2 μm × 2 μm. Right image size: 5 μm × 5 μm.

most of the film presents thicknesses between 10 and 18 nm, with an average value of 14 nm and a maximum value of around 23 nm. Taking into account the thickness measured for the LB film with one monolayer, a perfect layer-by-layer growth of 9 ML would lead to a film thickness of 20.7 nm. This means that these LB films reach the expected thickness but do not present a flat surface, due to incomplete coverage for each monolayer already shown after the transfer of the first monolayer.

AFM images of a LB film of **2** with one monolayer are shown in Figure 6. Circular domains with a diameter around 15 nm and a height of 2 nm appear on a flat surface (rms roughness ~ 0.25 nm). These higher domains present the expected height for the deposition of one monolayer, while the bottom surface exhibits a similar roughness to that of the naked substrate (0.2 nm). Furthermore, some zones of the surface are covered with higher domains of irregular shape with heights of around 4 and 6 nm. This might correspond to the transfer of bilayers and trilayers. When the number of monolayers is increased to 9, the whole surface is covered by an inhomogeneous film (rms roughness ~ 2.6 nm). An intermediate phase that presents some holes of irregular shape can be distinguished. The hole depth of 8 nm allows one to estimate the thickness of this intermediate phase (under the assumption that the substrate is still visible at the hole bottom). The rest of the film is mainly formed by domains with a height of 6 nm with respect to the intermediate phase. This indicates that the growth of the film does not take place in a complete regular way as already suggested by the images of the LB film with one monolayer and by the transfer ratios close to 0.6−0.7 calculated for both immersion and withdrawal of the substrate. There are few zones in which the film thickness overcomes 20 nm, but almost the whole film exhibits a thickness below 14 nm (with an average thickness of 10 nm). These values are lower than the expected height for 9 ML, taking into account that the thickness of the LB film with one monolayer is around 2 nm. As observed for the LB films of **1**, the uncompleted coverage for each monolayer leads to imperfect layer-by-layer growth of the films. In the case of LB films of **2**, this effect is even more evident and important, and therefore, the film is more discontinuous. In conclusion, the AFM analysis demonstrates the possibility to control the growth of multilayer films, although they do not show the expected thickness along the whole surface, especially in the case of **2**.

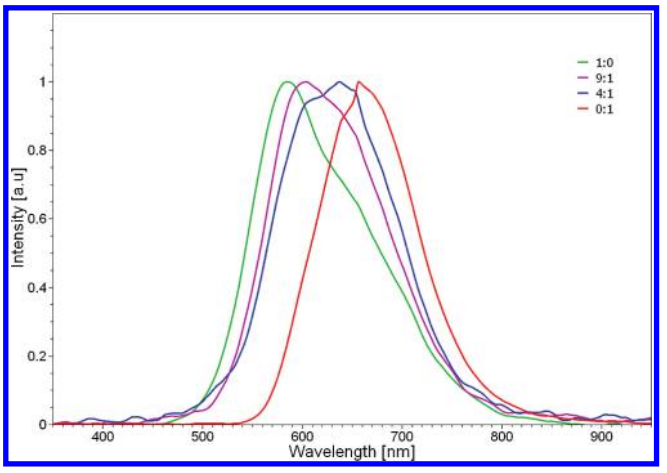

Figure 7. Normalized electroluminescence spectra for a series of ITO/pTPD/LB films of a mixture of **1** and **2** (30 ML)/Ba/Ag with ratios 1:0, 9:1, 4:1, and 0:1 of complex **2** and **1**, respectively, in the LB films.

Thickness Determination with a Profilometer. In addition to the AFM characterization of the LB films on glass substrates, the thickness of the LB films deposited on top of the pTPD layer within the devices was measured with a profilometer. The thickness of the LB film layer was calculated from the difference between the thickness of the double layer of pTPD plus the LB film and that of the pTPD layer alone that covers part of the substrate. Average thicknesses of a LB film of 30 ML of **1** deposited on top of the pTPD layer give a thickness per monolayer around 2.2 nm which is close to that obtained by AFM on glass substrates. On the other hand, a LB film of 30 ML of **2** on top of pTPD gives a thickness per monolayer close to 1.3 nm as a consequence of the worse surface coverage for transferred **2** monolayers shown by the low transfer ratios and by AFM measurements. Again, although the thickness of the LB films in the devices is smaller than the expected values for a perfect layer-by-layer growth in the case of **2**, this does not prevent a precise control of the thickness of both types of layers, which is the main advantage of the use of the LB technique for the preparation of these devices. The thickness per monolayer of the devices containing alternating LB films of **1** and **2** is decreasing at an increasing ratio of **2** monolayers as expected. Thus, the thickness per monolayer of the LB film layer formed by 10 ML of **2** and 30 ML of **1** is 1.95 nm, while that of the LB film with 4 ML of **1** and 26 ML of **2** is 1.76 nm.

Electroluminescence Properties of the Devices. Two reference devices were prepared using a multilayer of either compound **1** or **2**, with the architecture ITO/pTPD/LB Film/Ba/Ag. Upon applying an external voltage, current was flowing through the devices with a typical turn-on voltage of 1 to 2 V, for devices with compound **1** or **2**, respectively. At slightly higher voltages, the devices started to emit light (see Figure 6SS in the Supporting Information). The luminescence spectra obtained for both devices resemble those obtained by photoexcitation of the molecules in the LB film, indicating the complexes are the only source for the light generation.

To verify that it is possible to achieve emission from compound **1** in a matrix of compound **2**, devices with emission layers of mixed complexes were prepared. As observed from Figure 7, upon increasing the amount of compound **1**, the emission wavelength shifts toward the emission observed from a device with layers consisting of only compound **1**. In order to quantify this effect, the luminescence spectra of the devices containing **1** and **2** have been fitted to two Gaussians centered at 586 nm (emission from **2**) and 665 nm (emission from **1**). The relative intensity of the emission at 665 nm is around 50% of the sum of two intensities upon addition

of only 10% of **1** (see Figure 8SS in the Supporting Information). This demonstrates that the emission from **2** is transferred very efficiently to **1**. This effect is well-known and generally observed when an emissive molecule is introduced in a wider band gap host. In such a mixed system, either the electron and hole get trapped on the guest molecule and subsequently form an exciton on the guest molecule, or excitons generated on the host molecules are transferred to the guest molecules prior to their radiative decay, via either Foster or Dexter energy transfer.

A different device architecture has been studied as well resembling the architecture of multilayer vacuum processed OLEDs. It consists of bilayer devices of pure layers of compounds **1** and **2**. Taking advantage of the LB technology, two types of those devices were prepared: (A) several monolayers of compound **1** (20−30 ML) are deposited on top of several monolayers of compound **2** (4, 10, and 20 ML), (B) in which monolayers of compound **2** (20−26 ML) are deposited on top of monolayers of compound **1** (4 and 20 ML). Typical current density and luminance versus the applied bias are shown in Figure 7SS in the Supporting Information.

Interestingly, a spectral shift of the emission maximum is observed upon addition of monolayers of the complex **2**. First, the results obtained from the devices with structure A (with compound **1** deposited on top of compound **2**) will be discussed. Figure 8 shows the emission spectra obtained from the devices with a varying number of monolayers of compound **1** and **2**, including the reference devices having only either compound **1** or **2** as the active layer. Compared to the device using only compound **2**, upon addition of the same number of monolayers of compound **1** as the number of monolayers of compound **2**, the emission spectrum is broadened toward the red and appears to be the summation of the emission spectrum of compound **1** and that of compound **2**. Upon decreasing the amount of monolayers of compound **2** and, to maintain the total device thickness approximately the same, increasing amount of monolayers of compound **1**, the emission spectrum shifts further toward the red and seems to be based primarily on the emission spectrum of compound **1**. We have quantified this effect by fitting the emission spectra to two Gaussians centered at the emissions coming from **1** and **2** (see above). The relative intensity of **1** emission varies linearly with the fraction of monolayers of **1** (see Figure 8SS in the Supporting Information).

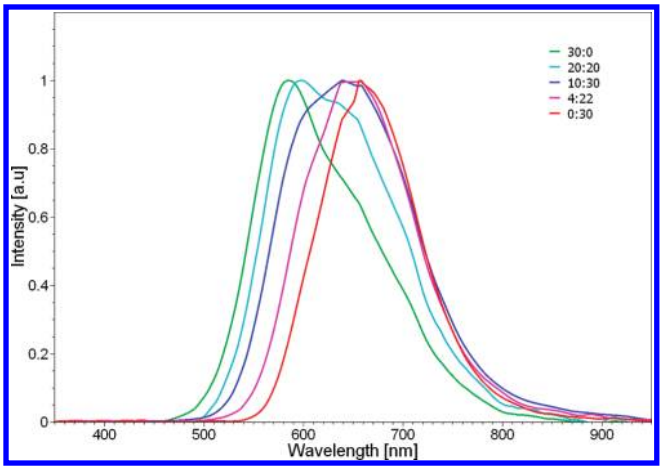

Figure 8. Normalized electroluminescence spectra for a series of ITO/pTPD/LB film of **2**/LB film of **1**/Ba/Ag with different numbers of monolayers of compound **2** and **1**, respectively; 30:0 (green), 20:20 (cyan), 10:30 (blue), 4:22 (pink), and 0:30 (red).

This observation can be understood by looking at the energy levels of the highest occupied molecular orbital (HOMO) and lowest unoccupied molecular orbital (LUMO) of the compounds and taking into account the long exciton lifetime of these phosphorescent complexes (microsecond range). A schematic presentation of the HOMO and LUMO levels for the materials used in these devices is depicted in Figure 9. In the case of compound **1** deposited on top of compound **2**, there is no barrier for holes to migrate from the monolayers of complex **2** into the monolayers of complex **1** nor is there a barrier for electrons to migrate from monolayers of complex **1** into the monolayers of complex **2**. Hence, recombination of holes and electrons can occur in both layers of complex **1** and layers of complex **2**. Therefore, upon increasing the number of monolayers of compound **1**, emission from complex **1** becomes more preponderant while emission from the monolayers of compound **2** still contributes to the overall emission of the device. There is an additional process occurring which is exciton transfer from the layer of compound **2** to the layer of compound **1** (see Figure 9). The magnitude of this transfer depends on the exciton diffusion length in the film. This appears to be in the order of the length of 4 ML, as in the device with this few monolayers of compound **2** there is hardly any contribution in the observed electroluminescent spectrum from compound **2**, indicating that practically all excitons are transferred to the layer of compound **1**. More monolayers of compound **2** result in an increased contribution of the overall emission of the device from compound **2**. In this configuration, the emission spectrum of the device can be tuned between the emission spectra of pure components simply by varying the relative number of monolayers of compounds **1** and **2**.

In the case of the devices with structure B (with compound **2** deposited on top of compound **1**), the situation is quite different. In this situation, easy transport of holes from the layer of compound **1** to compound **2** is not possible as the HOMO of compound **2** lies

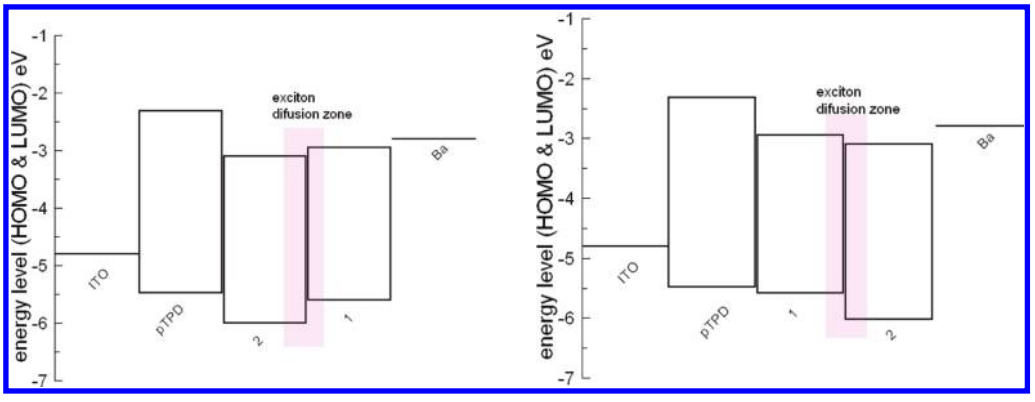

Figure 9. Schematic presentation of the HOMO and LUMO levels for the materials used in these devices with structure A (left) and structure B (right).

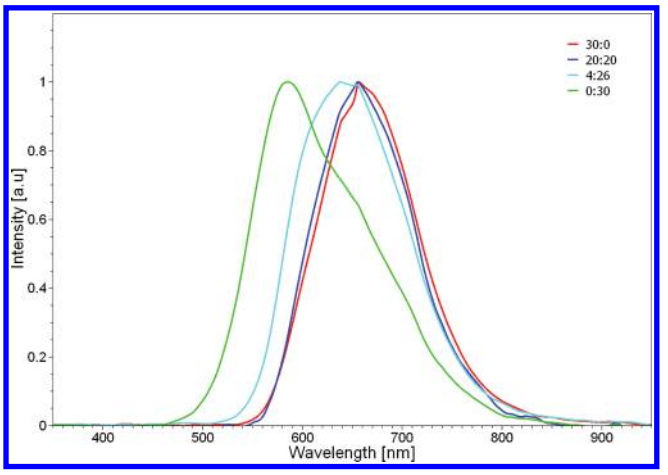

Figure 10. Normalized electroluminescence spectra for a series of ITO/pTPD/LB film of **1**/LB film of **2**/Ba/Ag with different numbers of monolayers of compound **1** and **2**, respectively; 30:0 (red), 20:20 (blue), 4:26 (cyan), and 0:30 (green).

well below the HOMO the compound **1** (Figure 9). Compound **2** acts as a hole-blocking layer. Additionally, since electrons are injected and transported efficiently through the layer of compound **2** as evidenced by the efficient emission from the underlying layer, it is likely that excitons in layer of **2** are predominantly generated close to the interface where they have a high probability to be transferred to molecules of compound **1**. Due to these effects, there is very little probability to obtain electroluminescence from compound **2**. This is observed in the case of the device with only 4 ML of compound **1**; even in this extreme case, there still is a strong contribution in the electroluminescent spectrum from compound **1** with only a minor contribution from compound **2** (see Figure 10). This is confirmed by the changes on the relative intensity of **1** with a fraction of monolayers of **1** (see Figure 8SS in the Supporting Information). The relative intensity of **1** in the device with only 4 ML of **1** is more than 70%.

As shown in Figure 9, the HOMO and LUMO levels of compound **1** do not entirely lie within the HOMO and LUMO gap of compound **2**, which allows for the migration of electrons from one layer to the other one. Holes on the contrary are efficiently blocked going from a layer consisting of compound **1** to a layer consisting of compound **2**. Furthermore, efficient transfer of excitons takes place from one layer to the other as evidenced by the appearance of the dual emission. A rough estimate concerning the exciton diffusion length in these LB films can also be made from the observation that practically all green emission disappeared when only 4 ML of compound **2** remain in device configuration A. This is done with the assumption that hole transport is slower in compound **2** than in compound **1**, whereas electron transport should be similar based on the difference in HOMO and LUMO levels and the fact that transport in these amorphous systems is frequently trap limited. The disappearance of green light emission indicates that all excitons that were generated in that layer are transferred to complexes of type **1** prior to their decay, and hence they must at least be able to move over the thickness of the layer containing compound **2** which is approximately 6 nm (one monolayer is 1.3 nm).

Conclusion

Dual emitting organic light-emitting diodes have been prepared using LB films of ionic ruthenium and iridium phosphorescent complexes. Dual emission was obtained by simple blending of the two emitters and by preparing a two stacked configuration, in which a LB layer of the ruthenium complexes was deposited on top of a LB layer of the iridium complexes and the inverse situation. Interestingly, the color can be tuned by the thickness of each LB layer. Due to efficient hole blocking of a layer of the iridium complexes when deposited on top of the layer of ruthenium complexes, in that configuration the green emission of the iridium complexes is suppressed. In the opposite case, excitons are generated in both layers although most likely preferentially in the layer of the iridium complexes. Also in this configuration, the green emission can be suppressed when the amount of LB layers decreases to approximately 4, giving a lower limit for the exciton diffusion length in this material. Finally, it is expected that, by using an iridium complex emitting in the blue part of the visible spectrum instead of the green part, white light-emitting devices would be obtained at low cost.

Acknowledgment. Financial support from the European Union (MolSpinQIP), the Spanish Ministerio de Ciencia e Innovación (Projects Consolider-Ingenio in Molecular Nanoscience, CSD2007-00010, and CTQ2008-06720), and the Generalitat Valenciana (Project PROMETEO/2008/128) is gratefully acknowledged.

Supporting Information Available: Additional figures with the compression isotherms of mixed **1** and **2** monolayers, BAM images, IR spectrum of the mixed **1** and **2** LB film, current density and luminance curves of the devices and relative emission of **1** and **2** in the devices are provided as supporting information. This material is available free of charge via the Internet at http://pubs.acs.org.